DFT Studies of Cubane [4Fe-4S]$^{2+/3+}$ Clusters: J-Aggregates of FeS Tetramers

Peshala K. Jayamaha, Grayson Venus, Cat Nimmo, Riya Krishnan, Zafeiria N. Nikolaidi, Zahid Siraj, and Lichang Wang*

School of Chemical and Biomolecular Sciences

Southern Illinois University Carbondale, Carbondale, IL 62901, USA

Abstract

Iron sulfur clusters are essential cofactors of numerous proteins that play many important biological roles due to their unique reactivity—a product of their geometry, oxidation, and spin states. The geometry of the iron sulfur clusters of [4Fe-4S]$^{2+}$ and [4Fe-4S]$^{3+}$ in various spin states was investigated using density functional theory (DFT). Geometry optimizations and vibrational frequency calculations were carried out on these clusters using the B3LYP functional and the 6-311+G(d,p) basis set. The most stable spin state for the [4Fe-4S]$^{2+}$ cluster was found to be the 19-et, an antisymmetric structure. The most stable spin state for the [4Fe-4S]$^{3+}$ cluster was found to be the 20-et, also an antisymmetric structure. Interestingly, these cubane clusters consist of J aggregates of four species of FeS and FeS^{+}. The breakage of a monomer FeS from a [4Fe-4S] cluster under different environments may be responsible for the observations of noncubane [4Fe-4S] clusters. Furthermore, with increased spin state, the positive and negative charges on the iron and sulfur increased and decreased, respectively, and the structure of cubane [4Fe-4S]$^{2+}$ cluster evolves from the structure with a Fe tetramer as core and S as ligands to J-aggregate of FeS and to a homogeneous [4Fe-4S]$^{2+}$ cluster.

* Corresponding author: lwang@chem.siu.edu

1. Introduction

Iron-sulfur clusters are the core structures that are found in the active site of many proteins and can appear in various sizes and shapes, including [Fe-4S], [2Fe-2S], [3Fe-4S], [4Fe-4S], and [8Fe-7S], as shown in Figure 1. These clusters are cofactors that are responsible for the activation of certain small molecules, are necessary for the normal function of the mitochondria, and are used in electron transfer, DNA repair, and other cell functions and have been used as electron reservoir or carrier for electron-transfer or redox reactions.[1-28] For instance, the involvement of Fe–S clusters in mitochondrial respiration links them to reactive oxygen species (ROS) production and oxygen sensing, with potential implications in diseases like pulmonary hypertension and mitochondrial disorders.[29]

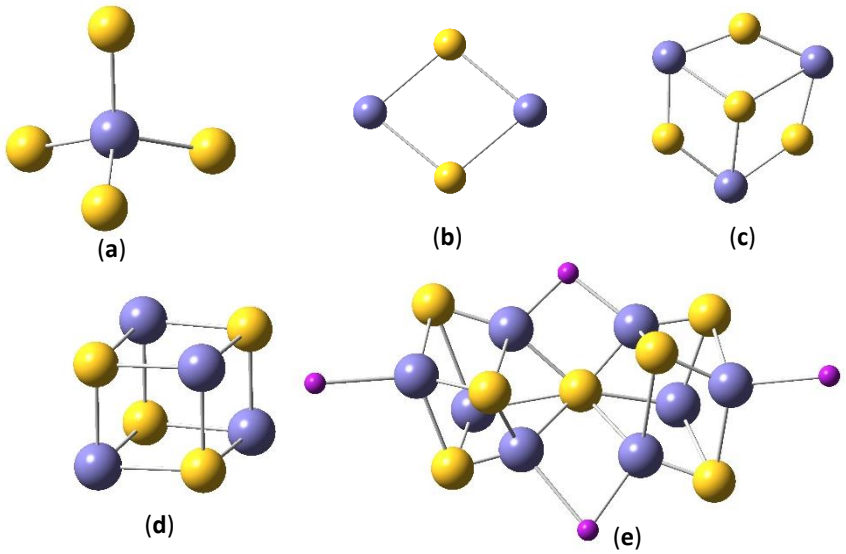

Figure 1. Core structures of iron-sulfur clusters in metalloproteins: (**a**) FeS_4 in rubredoxin; (**b**) [2Fe-2S] in plant-type ferredoxin; (**c**) [3Fe-3S] in bacterial ferredoxin; (d) [4Fe-4S] in bacterial ferredoxin and HiPIP, and (e) [8Fe-7S] with the purple balls=S for P cluster in MoFe proteins and the purple balls=N for synthesized inorganic cluster. Blue and yellow balls represent Fe and S, respectively.

The description of these clusters, established nearly 20 years ago, emphasizes their main elements, including ionic sizes, constant Fe−S bond distances, high-spin configurations, and

tetrahedral stereochemical preferences at Fe^{2+} and Fe^{3+} sites.[30] A large number of studies have been carried out on gas phase cationic,[31] neutral,[32] and anionic,[33-35] iron sulfur clusters for their composition, stability, and structure.[36-61] Iron-sulfur clusters often coordinate with cysteine residues in proteins. The sulfur atom in the thiol group of cysteine can coordinate with iron to form a stable coordination bond.[62] This interaction is crucial for the structure and function of many iron-sulfur cluster-containing proteins. The coordination of cysteine residues helps stabilize the iron-sulfur cluster within the protein structure.[63] Thus, iron-sulfur clusters are commonly found in living cells and are a worthwhile object of study. Recently, research was also done to incorporate Fe-S clusters in metal-organic frameworks to develop materials for gas adsorption.[64] Their unique reactivity is a product of their unique geometry, spin state, charge, and oxidation state.

Among the classes of iron–sulfur clusters shown in Figure 1, the [4Fe–4S] clusters are the most versatile.[39,53,65-67] The cubane-type [Fe4(μ3-S)4]n clusters play many roles in electron transfer, enzymatic catalysis, nitrogen fixation, photosynthesis, and gene regulation.[68] The coordination of iron and sulfur atoms in these clusters allows them to efficiently transfer electrons. The study of these clusters involves considering their redox states and the synthesis methods to gain insights into their structural and electronic features.[68] In the photoelectron spectroscopic studies of gaseous cubane [4Fe-4S] clusters of various charges, it was concluded that $[4Fe\text{-}4S]^-$ cluster is a two-layer spin-coupling structure.[61] To understand the mechanism of iron–sulfur clusters in various functions, study of their electronic structure and properties, such as spin states, is important.

Computational and theoretical chemistry has a very important role to play in helping to predict and rationalize the nature of the electronic ground state of transition metal compounds and understanding their electronic transfer properties and reactivity in proteins.[47,69-74] Among the many proteins containing an iron sulfur cluster, the iron-molybdenum cofactor of the molybdenum

nitrogenase enzyme, called FeMoco, is a well-studied molecule that contains an [4Fe-4S] cluster as its core. However, specific details about the oxidation states of the Fe, spin coupling, and spin localization remain unknown. These values likely play a key role in the reactivity of the cofactor. In the recent work by Benediktsson and Bjornsson, they used broken-symmetry density functional theory (DFT) in the ORCA quantum chemistry program to characterize these values to understand more about the cluster present in Femoco and determine the geometry.[75] Specifically, they looked at the functional dependence and electronic structural dependence of the molecule by using a test set of similar spin-coupled Fe-S systems.

Herein, we performed gas phase DFT calculations to evaluate and predict structural and electrical characteristics of cubane $[4Fe\text{-}4S]^{2+}$ and $[4Fe\text{-}4S]^{3+}$ clusters and compare the effect of spin state on the structural and electronic properties of these clusters. Particular attention was given to investigate what constitute the building blocks that form these cubane clusters. In this work, we employed B3LYP functional with a basis set of 6-311+G(d,p) in our calculations. Details of the choice of the method is discussed below.

2. Computational Details

Iron sulfur clusters [Fe4-S4] of spin states singlet/doublet to 22-et/23-et of the cationic +2 and +3 species, respectively, were evaluated using DFT calculations. Additionally, the first three spin states of FeS and FeS^+ and the first few spin states of Fe and S were evaluated. Each system was studied in the gas phase and was optimized to a minimum with a geometry optimization and the minima were confirmed via a subsequent vibrational frequency calculation.

All calculations were carried out in the ground state with unrestricted spin using the B3LYP functional and the 6-311+G(d,p) basis set. B3LYP has been used in the studies of Fe_2S_2 clusters[76]

and 6-311+G(d,p) was found to be a reasonably good basis set.[77] All calculations were conducted using the Gaussian16 program with GaussView 6[78] being used to generate the input files with all other parameters at default. From these calculations, the energies, optimized geometries, HOMO/LUMO, charge distribution, and IR spectrum of each system was obtained. Zero-point corrected energies were used in the calculation of the energies.

We note that all the structures are supposed to be at an energy minimum and no imaginary frequencies should exist. In a few calculations, efforts were made to remove the imaginary frequency without success. These structures with imaginary frequencies are reported in the results section.

3. Results and Discussion

In this work, we carried out DFT calculations to the two main clusters of interest, i.e. $[4Fe\text{-}4S]^{2+}$ and $[4Fe\text{-}4S]^{3+}$, at various spin states. To understand the structures and the building blocks of these clusters, we also carried out DFT calculations of Fe, S, FeS, and FeS^{+}, at various spin states. In what follows, we first present the results of $FeS^{0/+}$ followed by those of $[4Fe\text{-}4S]^{2+}$ and $[4Fe\text{-}4S]^{3+}$.

3.1 $FeS^{0/+}$ Species

The DFT results of various properties of FeS and FeS^{+} are summarized in Table 1. It is clear that the most stable spin state of FeS and FeS^{+} are quintet and sextet, respectively. To understand the bonding energy between Fe and S in FeS species, we also performed DFT calculations using B3LYP/6-311+G(d,p) for Fe at spin states of singlet, triplet, and quintet and S at spin state of singlet and triplet and used the lowest energy of the spin state. The bond energy of Fe-S is found to be 3.85 eV. Two interesting observations are the Fe-S bond length and charge distribution. To

compensate for higher spin, the Fe-S bond is lengthened and the species is more polarized with respect to the singlet state.

Table 1. Energies and other properties of FeS with different charges and spins

	Number of unpaired electrons	Energy* (eV)	Frequency (cm^{-1})	Bond length (A)	Mullikan charge Fe	S
FeS	0	2.76	566.6	1.944	0.186	-0.186
	2	0.68	376.0	2.109	0.180	-0.180
	4	0.00	512.4	2.035	0.275	-0.275
	6	1.00	440.6	2.115	0.080	-0.080
FeS^+	1	2.94	629.1	1.907	0.528	0.472
	3	0.21	426.1	2.109	0.669	0.331
	5	0.00	463.5	2.060	0.643	0.357

*The energy is relative to the most stable species.

3.2 $[4Fe\text{-}4S]^{2+}$ Species

DFT results of $[4Fe\text{-}4S]^{2+}$ clusters at various spins are summarized in Table 2. The most stable state was found with 18 unpaired electrons. If we decompose the unpaired number of electrons according to FeS and FeS^+, it consists of two FeS units and two FeS^+ units. Furthermore, the energy of $[4Fe\text{-}4S]^{2+}$ by binding these four units is 1.74 eV/$FeS^{0/-}$, which is nearly half of FeS bond energy. We note that this binding energy was calculated the same way as that in the previous studies of complex formation.[79] We performed further analysis based on the DFT results to support the above hypothesis and the discussion will be provided below.

Table 2. Energies and other properties of $[4Fe\text{-}4S]^{2+}$ with different spins

Label	Number of unpaired electrons	Energy* (eV)	HOMO energy (eV)	HOMO-LUMO gap (eV)	Number of and the imaginary frequencies (cm^{-1})	Mullikan charge Fe	S
a	0	6.23	-16.21	3.08	0	0.574	-0.074
b	2	6.42	-15.24	1.49	0	0.664	-0.164
c	4	5.51	-14.82	0.96	1 (-405.4)	0.679	-0.179
d	6	4.79	-14.70	0.99	0	-0.672	-0.172
e	8	3.49	-14.57	0.60	1 (-135.1)	0.68	-0.18
f	10	1.65	-14.57	0.65	1 (-708.7)	0.857	-0.357
g	12	1.33	-15.14	0.96	0	0.624	-0.357
h	14	0.85	-15.10	0.96	0	0.626	-0.126
i	16	0.84	-15.41	0.84	2 (-347.1, -347.0)	0.77	-0.27
j	18	0.00	-15.41	4.25	3 (-407.6, -253.1, -253.1)	0.871	-0.371
k	20	3.08	-	-	0	0.932	-0.432
l	22	6.05	-	-	2 (-312.6)	0.578	-0.078

Figure 2 shows the optimized structures of $[4Fe\text{-}4S]^{2+}$ with the most stable spin states (14, 16 and 18 unpaired electrons). All other geometries of $[4Fe\text{-}4S]^{2+}$ cluster show almost similar structures except slightly different Fe-S bond lengths and angles. All the relative energies associated with each geometry, HOMO-LUMO energies and Mullikan charges of atoms in each cluster are given in Table 2. The most stable electronic state of $[4Fe\text{-}4S]^{2+}$ cluster has 18 unpaired electrons, and the second lowest stable spin state (with 16 unpaired electrons) is 0.84 eV higher in energy. Spin states with 14 and 16 unpaired electrons are relatively close to each other in total energy. The relative energies of very low and high spin states are large compared to the most stable electronic structure of $[4Fe\text{-}4S]^{2+}$. According to the optimized structures, vertical Fe-S's act as subunits in the cluster and form a tetramer of Fe-S. According to the energies of each optimized structure, the 19-et spin state (with 18 unpaired electrons) has shown the lowest relative energy compared to the other spin states. However, it is associated with three imaginary frequencies which shows that this structure is not in a local minimum on the potential energy surface (PES). If there is one negative frequency it is a transition state which refers to the first-order saddle point. The positive charge of Fe atoms in the $[4Fe\text{-}4S]^{2+}$cluster increased with increasing spin state, while the charges of S atoms become more negative. The $[4Fe\text{-}4S]^{2+}$ cluster with +2 charge should be an antisymmetric structure according to the intensities in the IR spectra of $[4Fe\text{-}4S]^{2+}$. For the most stable $[4Fe\text{-}4S]^{2+}$ it is shown that Fe-S bond distance is increased through the low spin state to the higher spin state.

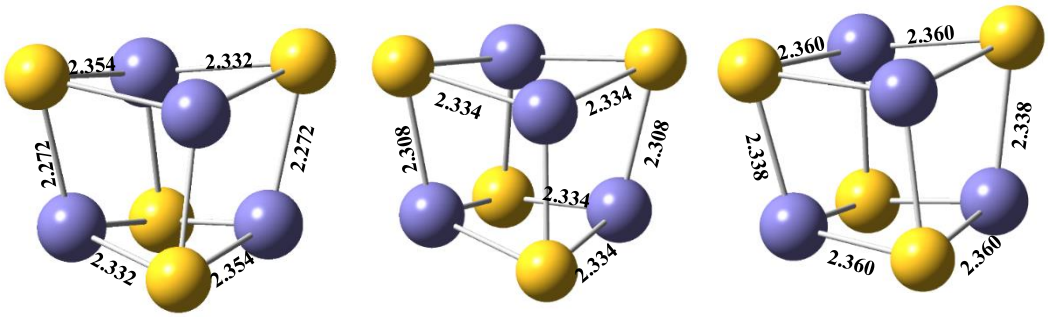

Figure 2. DFT optimized structures of $[4Fe\text{-}4S]^{2+}$ with the lowest energies shown in **Table 2**. The numbers are bond distances in Å.

Most interestingly, the structures shown in Figure 2 further support the conclusion about the building blocks (monomers) derived from the results based on the spin state and energy. Indeed, the bond distance in the four Fe-S building blocks is 2.338 Å, which is shorter than the bond distances between the monomers. Therefore, the formation of $[4Fe\text{-}4S]^{2+}$ is through a J aggregation, which has been found and studied in many applications.[80-82] Moreover, the charges among the monomers are evenly distributed after $[4Fe\text{-}4S]^{2+}$ formation where initially there are two monomers of FeS and two monomers of FeS^{+}. The concerted mechanism on iron-sulfur cluster assembly deduced from the most recent mass spectrometric studies[83] seems also to indicate the formation of FeS as building blocks (monomers). Finally, we mention that the three most stable isomers with different spin states can be identified using IR spectra. As shown in Figure 3, three signature IRs can be observed.

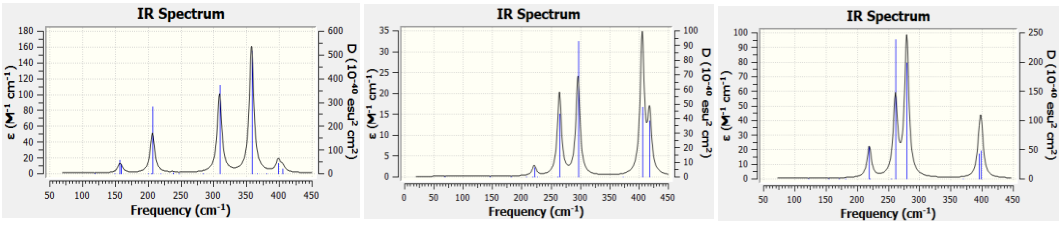

h **i** **j**

Figure 3. IR spectra for structure of $[4Fe\text{-}4S]^{2+}$ with the lowest energies, shown in **Table 2**.

Figure 4 visualizes the electron distribution of frontier molecular orbitals of the most stable $[4Fe\text{-}4S]^{2+}$ clusters. The energy difference between HOMO-LUMO levels of the most stable $[4Fe\text{-}4S]^{2+}$ cluster (with 18 unpaired electrons) is 4.25 eV. There are visible differences among the molecular contours, but those of structure **h** and **i** show great resemblance. We note that the interpretation of the small HOMO-LUMO energy gap in these high spin clusters needs to be cautious as the B3LYP functional's ability to deal accurately with strong coupling systems. The strong coupling systems like these clusters need to be further investigated by considering adding an on-site Coulomb repulsion, or U term, to correct the underestimation of HOMO-LUMO energy gap.[84]

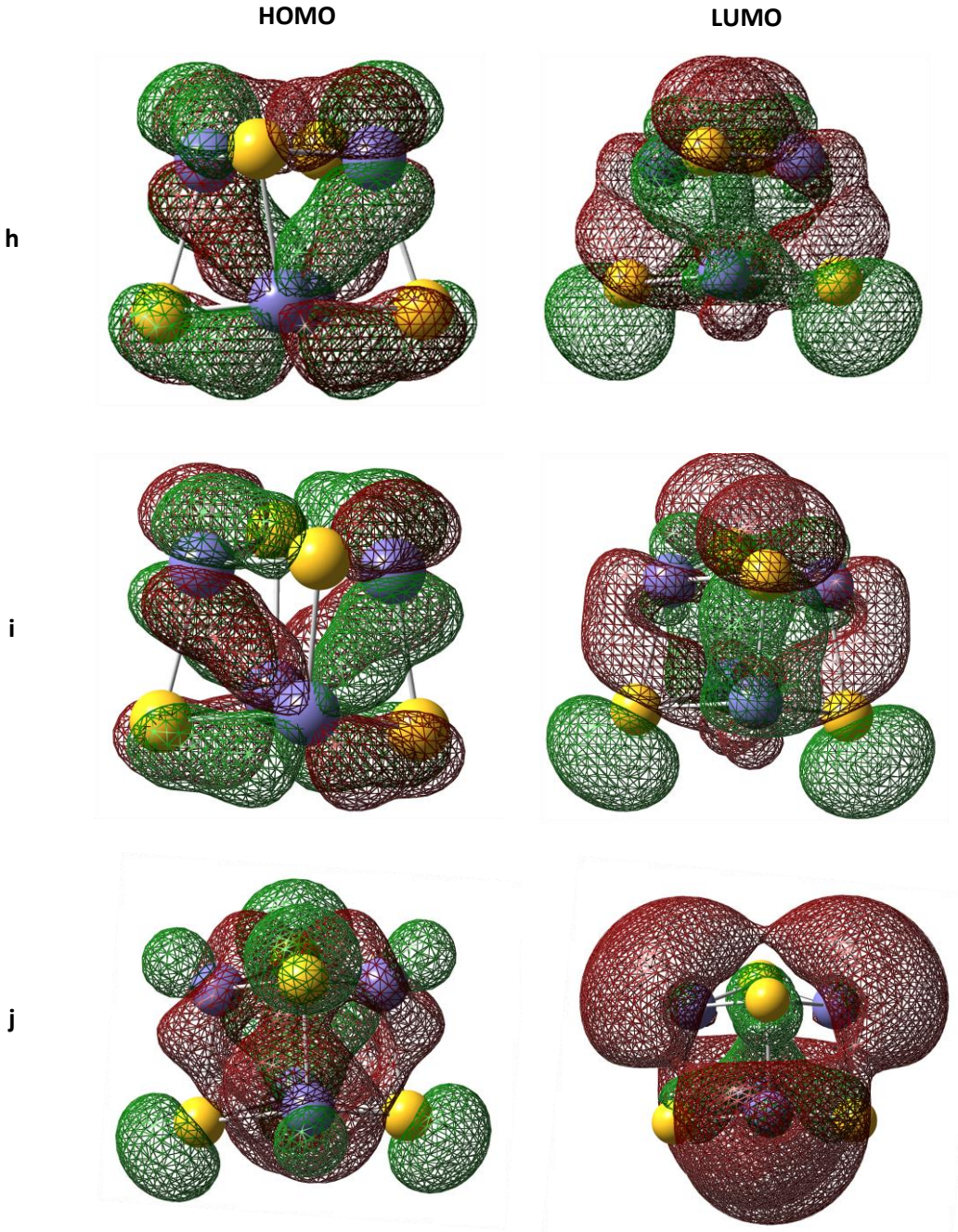

Figure 4. Frontier molecular orbitals (HOMO and LUMO) of $[4Fe\text{-}4S]^{2+}$ with the lowest energies, shown in **Table 2**.

3.3 $[4Fe\text{-}4S]^{3+}$ Species

The DFT results for the $[4Fe\text{-}4S]^{3+}$ clusters are summarized in Table 3. Structure j with 19 unpaired electrons is the most stable. The relative energy difference between the second (17 unpaired electrons) and third (15 unpaired electrons) most stable electronic structure is 0.57 eV. When scanned from lower (doublet) to higher spin states (22-et), the relative energy starts at higher in energy (5.98 eV) and achieves to a minimum (in 20-et) and starts to increase again (2.44 eV). The three most stable optimized structures of $[4Fe\text{-}4S]^{3+}$ clusters are shown in Figure 5. All Fe-S bond distances in the highest stable spin state (**i**, with 19 unpaired electrons) of the plus three cluster show the same value (2.385 Å), indicating it is likely a more cubic structure compared to the other two structures.

Table 3. Energies and other properties of $[4Fe\text{-}4S]^{3+}$ with different spins

Label	Number of unpaired electrons	Energy* (eV)	HOMO energy (eV)	HOMO-LUMO gap (eV)	Number of imaginary frequencies (cm^{-1})	Mullikan charge Fe	Mullikan charge S
a	1	5.98	-20.48	1.61	0	0.729	0.021
b	3	6.12	-20.23	1.24	0	0.708	0.042
c	7	3.54	-18.89	-0.02	0	0.959	-0.209
d	9	1.62	-19.58	0.71	0	0.933	-0.183
e	11	1.63	-19.56	0.49	0	0.905	-0.155
f	13	0.97	-19.64	0.82	0	0.803	-0.053
g	15	0.82	-19.56	0.95	0	0.915	-0.165
h	17	0.25	-19.81	0.73	2 (-478.2, -478.0)	0.993	-0.243
i	19	0.00	-19.79	4.23	0	1.033	-0.283
j	22	2.44	-	-	0	0.802	-0.052

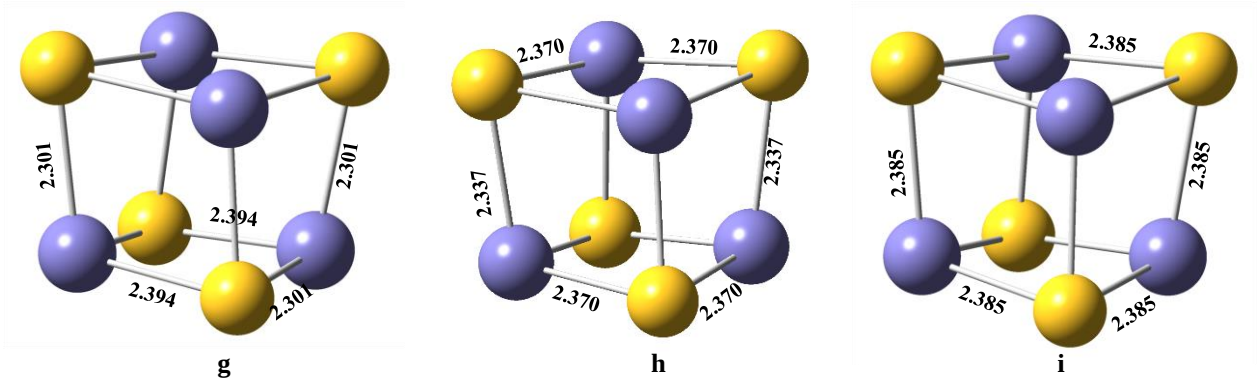

Figure 5. DFT optimized structures of $[4Fe\text{-}4S]^{3+}$ with the lowest energies, shown in **Table 3**. The numbers are bond distances in Å.

The three most stable $[4Fe\text{-}4S]^{3+}$ clusters also exhibited the antisymmetric structure according to the IR intensities (Figure 6). However, these clusters should be more symmetric than the $[4Fe\text{-}4S]^{2+}$ clusters with low IR intensities (with comparison between Figure 3 and Figure 6). Results show that removal of one electron from $[4Fe\text{-}4S]^{3+}$ increases the cluster symmetry. The energy difference between HOMO-LUMO levels of the most stable $[4Fe\text{-}4S]^{3+}$ cluster (20-et) is 4.23 eV. The HOMO-LUMO energy gap is relatively similar in most stable $[4Fe\text{-}4S]^{3+}$ and the $[4Fe\text{-}4S]^{2+}$ clusters. This higher frontier orbital gaps in stable states of $[4Fe\text{-}4S]^{3+/2+}$ implies that their low chemical reactivity and high kinetic stability[85] compared to other spin states.

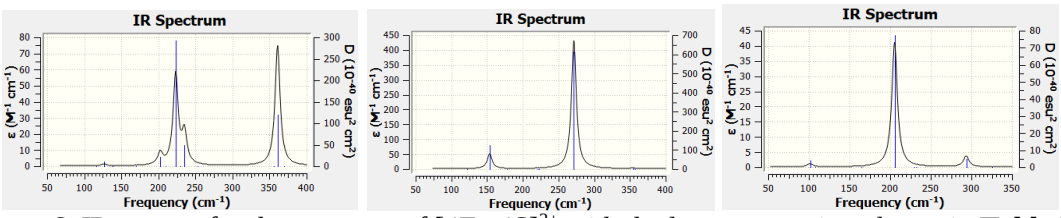

Figure 6. IR spectra for the structure of $[4Fe\text{-}4S]^{3+}$ with the lowest energies, shown in **Table 3**.

The frontier molecular orbitals of the three most stable clusters of $[4Fe\text{-}4S]^{3+}$ are depicted in Figure 7. There are more apparent differences among the orbitals of these clusters in comparison to the three $[4Fe\text{-}4S]^{2+}$ clusters. The delocalization character of the unpaired electron can be seen clearly.

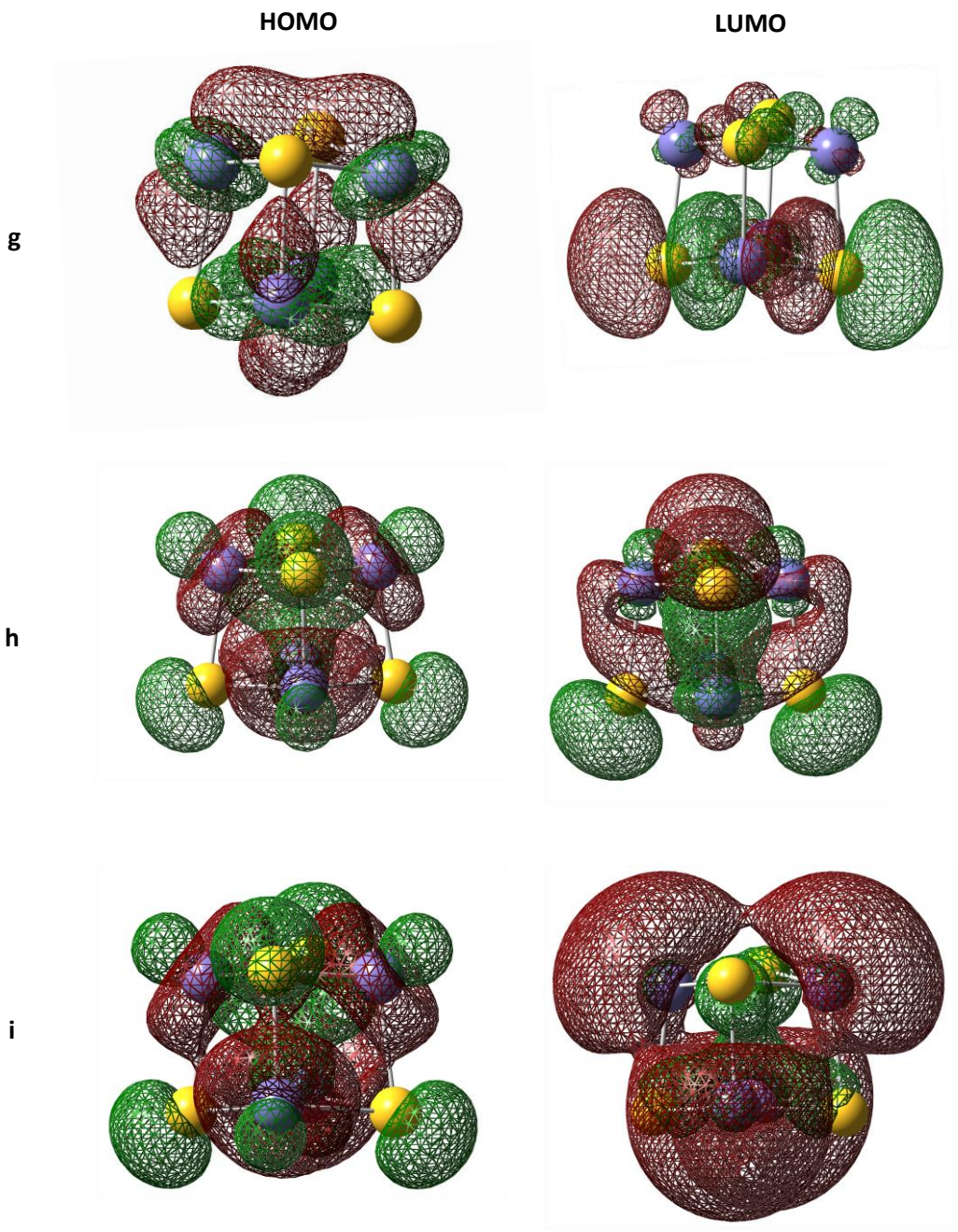

Figure 7. Frontier molecular orbitals (HOMO and LUMO) of $[4Fe\text{-}4S]^{3+}$ with the lowest energies, shown in **Table 3**.

3.4 Discussion

Figure 8 shows the singlet $[4Fe\text{-}4S]^{2+}$ and doublet $[4Fe\text{-}4S]^{3+}$, which are the lowest spin states of the corresponding clusters. These low spin clusters are different and we expect they will function differently in the adsorption of gas phase molecules than the high spin clusters.[86] For the singlet $[4Fe\text{-}4S]^{2+}$, it does no longer resemble the J aggregates of FeS at high spin states. Rather, it is a tetramer Fe cluster (Fe_4) ligated with an S atom on each surface. We expect this cluster will resemble more on the metal cluster and ligand effects of transition metal clusters.[87-89] Analysis of structures obtained from the current studies indicates that spin state is a good modulator to the structural changes of [4Fe-4S] clusters. At lower spin, $[4Fe\text{-}4S]^{2+}$ is a structure consisting of a metal cluster core with S as ligands as shown in Figure 8. When spin increases, it becomes a J-aggregate of FeS with a further increase of spin state, it becomes homogeneous [4Fe-4S] cluster, i.e. all the bond distances between Fe and S are the same. Furthermore, upon removing an electron from singlet $[4Fe\text{-}4S]^{2+}$, the metal core in the cluster breaks and it becomes a J-aggregate of the FeS tetramer, as shown in Figure 8 in doublet $[4Fe\text{-}4S]^{3+}$.

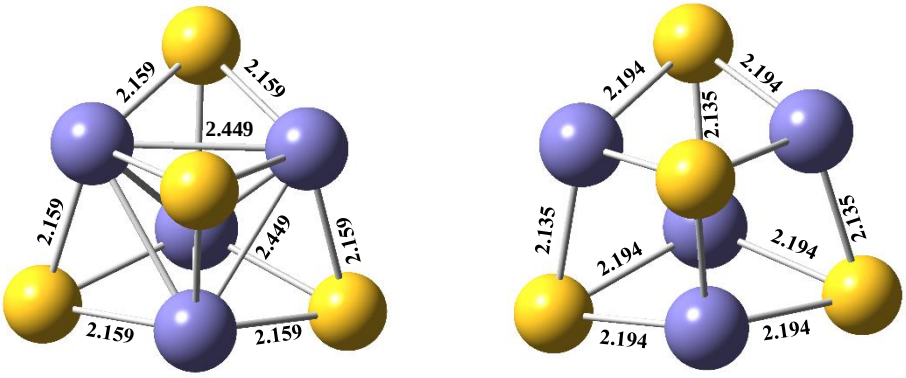

$[4Fe\text{-}4S]^{2+}$ $[4Fe\text{-}4S]^{3+}$

Figure 8. DFT optimized structures: singlet of $[4Fe\text{-}4S]^{2+}$ and doublet of $[4Fe\text{-}4S]^{3+}$.

For the most stable clusters, the J aggregates will behavior differently and have different internally built-in field[90] with respect to the clusters shown in Figure 8. These may be observed from electron excitation. Understanding the excited state of materials,[91-95] tuning excitons,[96-102] and coherent state control[103] have been active research. The clusters discussed here with higher spin states seem to have the characteristic of forming coherent states and therefore exhibiting longer exciton relaxation. This is a topic of enormous importance.

Iron-sulfur clusters are important metal cofactors in enzymes,[104,105] making them of utmost importance in the industrial and biochemical catalysis field.[3,105] These clusters have crucial roles in various biological processes including energy conversion,[106] nitrogen fixation,[107] DNA maintenance,[108] signal transduction,[109] redox regulation,[110] and biological catalysis.[111] Therefore, the current studies are important to the understanding of FeS clusters and may shed light on other catalysis research on important reactions,[112-118] including our current interest in ethanol oxidation[84,119-125] and catalyst properties.[126-128] Finally, we point out that broken-symmetry DFT (BS-DFT) studies of the clusters are essential before any further studies, as the comparison of results between DFT and BS-DFT calculations indicates that it is necessary to carry out such a study.[129-134] The current results can serve as a benchmark for future BS-DFT studies.

4 Conclusions

The gas phase DFT calculations using B3LYP/6-311+G(d,p) were performed to obtain the structural parameters and properties of $[4Fe\text{-}4S]^{2+}$ and $[4Fe\text{-}4S]^{3+}$ clusters. The most stable spin state for $[4Fe\text{-}4S]^{2+}$ cluster is the 19-et (18 unpaired electrons), while it is the 20-et state (19 unpaired electrons) for $[4Fe\text{-}4S]^{3+}$. IR intensities of both clusters implied that the removal of one electron increases the cluster symmetry, as $[4Fe\text{-}4S]^{3+}$ exhibited a more symmetric structure than

$[4Fe\text{-}4S]^{2+}$. The stable states of both [4Fe-4S] clusters have higher kinetic stability compared to their other spin states.

The most stable cubane $[4Fe\text{-}4S]^{2+}$ and $[4Fe\text{-}4S]^{3+}$ clusters can be considered the J aggregates of $FeS^{0/+}$ tetramers with strong electrostatic interactions among the tetramers. The change of environments can distort the cubane structure and lead to the formation of noncubane structures with displacement of a monomer FeS and may be used to understand the observations of the noncubane [4Fe-4S] clusters. Finally, the DFT results reported here can also serve as benchmark for future BS-DFT calculations.

References

(1) Shoji, M.; Koizumi, K.; Kitagawa, Y.; Yamanaka, S.; Kawakami, T.; Okumura, M.; Yamaguchi, K. *Int. J. Quantum. Chem.* **2005**, *105*, 628.
(2) Hori, Y.; Sato, A.; Shigeta, Y. *J. Comput. Chem. Jpn.* **2022**, *21*, 77.
(3) Rees, D. C.; Howard, J. B. *Science* **2003**, *300*, 929.
(4) Prakash, D.; Walters, K. A.; Martinie, R. J.; McCarver, A. C.; Kumar, A. K.; Lessner, D. J.; Krebs, C.; Golbeck, J. H.; Ferry, J. G. *J. Biol. Chem.* **2018**, *293*, 9198.
(5) Beinert, H. *J. Biol. Inorg. Chem.* **2000**, *5*, 2.
(6) Čorić, I.; Mercado, B. Q.; Bill, E.; Vinyard, D. J.; Holland, P. L. *Nature* **2015**, *526*, 96.
(7) Pandey, A. K.; Pain, J.; Dancis, A.; Pain, D. *J. Biol. Chem.* **2019**, *294*, 9489.
(8) Meyer, J. *J. Biol. Inorg. Chem.* **2007**, *13*, 157.
(9) Yang, H.; Impano, S.; Shepard, E. M.; James, C. D.; Broderick, W. E.; Broderick, J. B.; Hoffman, B. M. *J. Am. Chem. Soc.* **2019**, *141*, 16117.
(10) Seefeldt, L. C.; Yang, Z.-Y.; Lukoyanov, D. A.; Harris, D. F.; Dennis R. Dean; Raugei, S.; Hoffman, B. M. *Chem. Rev.* **2020**, *120*, 5082.
(11) Mao, Z.; Liou, S.-H.; Khadka, N.; Francis E. Jenney, J.; Goodin, D. B.; Seefeldt, L. C.; Adams, M. W. W.; Cramer, S. P.; Larsen, D. S. *Biochem.* **2019**, *57*, 978.
(12) Lill, R.; Muhlenhoff, U. *Trends in Biochem. Sci.* **2005**, *30*, 133.
(13) Crack, J. C.; Green, J.; Thomson, A. J.; Brun, N. E. L. *Acct. Chem. Res.* **2014**, *47*, 3196.
(14) Shi, R.; Hou, W.; Wang, Z.-Q.; Xu, X. *Front. Cell Develop. Biol.* **2021**, *9*, 735678.
(15) Saka, A.; Jule, L. T.; Soressa, S.; Gudata, L.; Nagaprasad, N.; Seenivasan, V.; Ramaswamy, K. *Sci. Rep.* **2022**, *12*, 10486.
(16) Pfaffen, S.; Abdulqadir, R.; Brun, N. E. L.; Murphy, M. E. P. *J. Biol. Chem.* **2013**, *288*, 14917.
(17) Zhang, B.; Crack, J. C.; Subramanian, S.; Green, J.; Thomson, A. J.; Brun, N. E. L.; Johnsona, M. K. *PNAS* **2012**, *109*, 15734.
(18) Wan, T.; Li, S.; Beltran, D. G.; Schacht, A.; Zhang, L.; Becker, D. F.; Zhang, L. *Nuclei Acids Res.* **2020**, *48*, 501.
(19) Fenwick, M. K.; Mehta, A. P.; Zhang, Y.; Abdelwahed, S. H.; Begley, T. P.; Ealick, S. E. *Nat. Commun.* **2015**, *6*, 6480.
(20) Wei, Y.; Li, B.; Prakash, D.; Ferry, J. G.; Elliott, S. J.; Stubbe, J. *Biochem.* **2015**, *54*, 7019.
(21) Gauhan, S. J. H.; Hirst, J. D.; Croft, A. K.; Jager, C. M. *J. Chem. Inf. Model.* **2022**, *62*, 591.

(22) Crooks, D. R.; Maio, N.; Lane, A. N.; Jarnik, M.; Higashi, R. M.; Haller, R. G.; Yang, Y.; Fan, T. W.-M.; Linehan, W. M.; Rouault, T. A. *J. Biol. Chem.* **2018**, *293*, 8297.
(23) Jordan, S. F.; Ioannou, I.; Rammu, H.; Halpern, A.; Bogart, L. K.; Ahn, M.; Vasiliadou, R.; Christodoulou, J.; Maréchal, A.; Lane, N. *Nat. Commun.* **2021**, *12*, 5925.
(24) Ebrahimi, K. H.; Ciofi-Baffoni, S.; Hagedoorn, P.-L.; Nicolet, Y.; Brun, N. E. L.; Hagen, W. R.; Armstrong, F. A. *Nat. Chem.* **2022**, *14*, 253.
(25) Thiriveedi, V. R.; Mattam, U.; Pattabhi, P.; Bisoyi, V.; Talari, N. K.; Krishnamoorthy, T.; Sepuri, N. B. V. *Redox Biol.* **2020**, *37*, 101725.
(26) Pandelia, M.-E.; Nitschke, W.; Infossi, P.; Giudici-Orticoni, M.-T.; Bill, E.; Lubitz, W. *PNAS* **2011**, *108*, 6097.
(27) Shaodong Dai1, R. F.; Glauser, D. A.; Bourquin, F.; Manieri, W.; Schu¨rmann, P.; Eklund, H. *Nature* **2007**, *448*, 92.
(28) Schurmann, P.; Buchanan, B. B. *Antioxidants Redox Signaling* **2008**, *10*, 1235.
(29) Read, A. D.; Bentley, R. E.; Archer, S. L.; Dunham-Snary, K. J. *Redox Biol.* **2021**, *47*, 102164.
(30) Holm, R. H.; Lo, W. *Chem. Rev.* **2016**, *116*, 13685.
(31) Koszinowski, K. S. d., D.; Schwarz, H.; Liyanage, R.; Armentrout, P. B. *J. Chem. Phys.* **2002**, *117*, 10039−10056.
(32) Yin, S.; Wang, Z. C.; Bernstein, E. R. *Phys. Chem. Chem. Phys.* **2013**, *15*, 4699−4706.
(33) Zhang, N.; Hayase, T.; Kawamata, H.; Nakao, K.; Nakajima, A.; Kaya, K. *J. Chem. Phys.* **1996**, *104*, 3413−3419.
(34) Zhai, H.-J.; Kiran, B.; Wang, L.-S. *J. Phys. Chem. A* **2003**, *107*, 2821.
(35) Yin, S.; Bernstein, E. R. *J. Phys. Chem. A* **2017**, *121*, 7362.
(36) Schmøkel, M. S.; Bjerg, L.; Cenedese, S.; Jørgensen, M. R. V.; Chen, Y.-S.; Overgaard, J.; Iversen, B. B. *Chem. Sci.* **2014**, *5*, 1408.
(37) Mouesca, J.-M.; Lamotte, B. *Coord. Chem. Rev.* **1998**, *178-180*, 1573.
(38) Kilpatrick, L. K.; Kennedy, M. C.; Beinert, H.; Czernuszewicz, R. S.; Spiro, T. G.; Qiu, D. *J. Am. Chem. Soc.* **1994**, *116*, 4053.
(39) Jafari, S.; Ryde, U.; Irani, M. *Sci. Rep.* **2023**, *13*, 10832.
(40) Ali, F.; Shafaa, M. W.; Amin, M. *Biology* **2022**, *11*, 362.
(41) Carvalho, A. T. P.; Swart, M. *J. Chem. Inf. Model.* **2014**, *54*, 613.
(42) Caserta, G.; Zuccarello, L.; Barbosa, C.; Silveira, C. M.; Moe, E.; Katz, S.; Hildebrandt, P.; Zebger, I.; Todorovic, S. *Coord. Chem. Rev.* **2022**, *452*, 214287.
(43) Valer, L.; Rossetto, D.; Scintilla, S.; Hu, Y. J.; Tomar, A.; Nader, S.; Betinol, I. O.; Mansy, S. S. *Can. J. Chem.* **2022**, *100*, 475.
(44) Noodleman, L.; Peng, C. Y.; Case, D. A.; Mouesca, J. M. *Coord. Chem. Rev.* **1995**, *144*, 199.
(45) Wang, X. B.; Niu, S.; Yang, X.; Ibrahim, S. K.; Pickett, C. J.; Ichiye, T.; Wang, L. S. *J. Am. Chem. Soc.* **2003**, *125*, 14072.
(46) Hirano, Y.; Takeda, K.; Miki, K. *Nature* **2016**, *534*, 281.
(47) Era, I.; Kitagawa, Y.; Yasuda, N.; Kamimura, T.; Amamizu, N.; Sato, H.; Cho, K.; Okumura, M.; Nakano, M. *Molecules* **2021**, *26*, 6129.
(48) Johnson, D. C.; Dean, D. R.; Smith, A. D.; Johnson, M. K. *Annu. Rev. Biochem.* **2005**, *74*, 247.
(49) Wachnowsky, C.; Hendricks, A. L.; Wesley, N. A.; Ferguson, C.; Fidai, I.; Cowan, J. *Inorg. Chem.* **2019**, *58*, 13686.
(50) Strop, P.; Takahara, P. M.; Chiu, H.-J.; Angove, H. C.; Burgess, B. K.; Rees, D. C. *Biochem.* **2001**, *40*, 651.
(51) Niu, S.; Wang, X.-B.; Yang, X.; Wang, L.-S.; Ichiye, T. *J. Phys. Chem. A* **2004**, *108* 6750.
(52) Mitra, D.; George, S. J.; Guo, Y.; Kamali, S.; Keable, S.; Peters, J. W.; Pelmenschikov, V.; Case, D. A.; Cramer, S. P. *J. Am. Chem. Soc.* **2013**, *135*, 2530.

(53) Pelmenschikov, V.; Ferreira, D.; Venceslau, S. S.; Hildebrandt, P.; Pereira, I. A.; Todorovic, S. *J. Am. Chem. Soc.* **2022**, *145*, 7.
(54) Yuan, Y.; Wang, L.; Gao, L. *Front. Chem.* **2020**, *8*, 818.
(55) Cracka, J. C.; Thomsona, A. J.; Brun, N. E. L. *PNAS* **2017**, E3215.
(56) Crow, A.; Lawson, T. L.; Lewin, A.; Moore, G. R.; Brun, N. E. L. *J. Am. Chem. Soc.* **2009**, *131*, 6808.
(57) Crack, J. C.; Gaskell, A. A.; Green, J.; Cheesman, M. R.; Brun, N. E. L.; Thomson, A. J. *J. Am. Chem. Soc.* **2008**, *130*, 1749.
(58) Crack, J. C.; Green, J.; Cheesman, M. R.; Brun, N. E. L.; Thomson, A. J. *PNAS* **2007**, *104*, 2092.
(59) Ohnishi, T. *Biochimica et Biophysica Acta (BBA)* **1998**, *1364*, 186.
(60) Jameson, G. N. L.; Walters, E. M.; Manieri, W.; Schurmann, P.; Johnson, M. K.; Huynh, B. H. *J. Am. Chem. Soc.* **2003**, *125*, 1146.
(61) Zhai, H.-J.; Yang, X.; Fu, Y.-J.; Wang, X.-B.; Wang, L.-S. *J. Am. Chem. Soc.* **2004**, *126*, 8413.
(62) Shepard, E. M.; Broderick, J. M. *8.17 - S-Adenosylmethionine and Iron–Sulfur Clusters*; Elsevier, 2010.
(63) Jagannathan, B.; Golbeck, J. H. *FX, FA, and FB Iron–Sulfur Clusters in Type I Photosynthetic Reaction Centers, Encyclopedia of Biological Chemistry*; Second ed.; Academic Press, 2013.
(64) Keshavarz, F.; Rezaei, N.; Barbiellini, B. *Langmuir* **2023**, *39*, 389.
(65) Brown, A. C.; Thompson, N. B.; Suess, D. L. M. *J. Am. Chem. Soc.* **2022**, *144*, 9066.
(66) Wagner, T.; Koch, J.; Ermler, U.; Shima, S. *Science* **2017**, *357*, 699.
(67) Wu, J.; Chen, S.-L. *ACS Catal.* **2022**, *12*, 2606.
(68) Lee, S. C.; Lo, W.; Holm, R. H. *Chem. Rev.* **2014**, *114*, 3579.
(69) Johnson, M. K. *Current Opioion Chem. Biol.* **1998**, *2*, 173.
(70) Szilagyi, R. K.; Winslow, M. A. *J. Comput. Chem.* **2006**, *27*, 1385.
(71) Nanda, V., Senn, S.; Pike, D. H.; Rodriguez-Granillo, A.; Hansen, W. A.; Khare, S. D.; Noy, D. *Biochimica et Biophysica Acta (BBA) - Bioenergetics*, **2016**, *1857*, 531.
(72) Torres, R. A.; Lovell, T.; Noodleman, L.; Case, D. A. *J. Am. Chem. Soc.* **2003**, *125*, 1923.
(73) Sandala, G. M.; Hopmann, K. H.; Ghosh, A.; Noodleman, L. *J. Chem. Theory Comput.* **2011**, *7*, 3232.
(74) Jodts, R. J.; Wittkop, M.; Ho, M. B.; Broderick, W. E.; Broderick, J. B.; Hoffman, B. M.; Mosquera, M. A. *J. Am. Chem. Soc.* **2023**, *145*, 13879.
(75) Benediktsson, B.; Bjornsson, R. *J. Chem. Theory Comput.* **2022**, *18*, 1437.
(76) Hubner, O.; Sauer, J. *Phys. Chem. Chem. Phys.* **2002**, *4*, 5234.
(77) Perera, S. M.; Aikawa, T.; Shaner, S. E.; Moran, S. D.; Wang, L. *J. Phys. Chem. A* **2023**, *127*, 8911.
(78) M. J. Frisch, G. W. T., H. B. Schlegel, G. E. Scuseria, M. A. Robb, J. R. Cheeseman, G. Scalmani, V. Barone, G. A. Petersson, H. Nakatsuji, X. Li, M. Caricato, A. V. Marenich, J. Bloino, B. G. Janesko, R. Gomperts, B. Mennucci, H. P. Hratchian, J. V. Ortiz, A. F. Izmaylov, J. L. Sonnenberg, D. Williams-Young, F. Ding, F. Lipparini, F. Egidi, J. Goings, B. Peng, A. Petrone, T. Henderson, D. Ranasinghe, V. G. Zakrzewski, J. Gao, N. Rega, G. Zheng, W. Liang, M. Hada, M. Ehara, K. Toyota, R. Fukuda, J. Hasegawa, M. Ishida, T. Nakajima, Y. Honda, O. Kitao, H. Nakai, T. Vreven, K. Throssell, J. A. Montgomery, Jr., J. E. Peralta, F. Ogliaro, M. J. Bearpark, J. J. Heyd, E. N. Brothers, K. N. Kudin, V. N. Staroverov, T. A. Keith, R. Kobayashi, J. Normand, K. Raghavachari, A. P. Rendell, J. C. Burant, S. S. Iyengar, J. Tomasi, M. Cossi, J. M. Millam, M. Klene, C. Adamo, R. Cammi, J. W. Ochterski, R. L. Martin, K. Morokuma, O. Farkas, J. B. Foresman, and D. J. Fox *Gaussian, Inc., Wallingford CT* **2016**.
(79) Lin, T.; Zhang, W.; Wang, L. *J. Phys. Chem. A* **2008**, *112*, 13600.
(80) Xu, F.; Testoff, T. T.; Wang, L.; Zhou, X. *Molecules* **2020**, *25*, 4478.

(81) Xu, F.; Gong, K.; Fan, W.; Liu, D.; Li, W.; Wang, L.; Zhou, X. *ACS Appl. Energy Mater.* **2022**, *5*, 13780.
(82) Testoff, T. T.; Aikawa, T.; Tsung, E.; Lesko, E.; Wang, L. *Chem. Phys.* **2022**, *562*, 111641.
(83) Bennett, S. P.; Crack, J. C.; Puglisi, R.; Pastore, A.; Brun, N. E. L. *Chem. Sci.* **2023**, *14*, 78.
(84) Xu, H.; Miao, B.; Zhang, M.; Chen, Y.; Wang, L. *Phys. Chem. Chem. Phys.* **2017**, *19*, 26210.
(85) Miar, M. S., A.; Pourshamsian, K.; Oliaey, A. R.; Hatamjafari, F. *J. Chem. Res.* **2021**, *45* 147.
(86) Amitouche, F.; Saad, F.; Tazibt, S.; Bouarab, S.; Vega, A. s. *J. Phys. Chem. A* **2019**, *123*, 10919.
(87) Lu, J.; Aydin, C.; Browning, N. D.; Wang, L.; Gates, B. C. *Catal. Lett.* **2012**, *142*, 1445.
(88) Spivey, K.; Williams, J. I.; Wang, L. *Chem. Phys. Lett.* **2006**, *432*, 163.
(89) Wang, L.; Williams, J. I.; Lin, T.; Zhong, C. J. *Catal. Today* **2011**, *165*, 150.
(90) Fan, X.; Wu, Z.; Wang, L.; Wang, C. *Chem. Mater.* **2017**, *29*, 639.
(91) Gong, K.; Yang, J.; Testoff, T. T.; Li, W.; Wang, T.; Liu, D.; Zhou, X.; Wang, L. *Chem. Phys.* **2021**, *549*, 111256.
(92) Wang, T.; Zhao, C.; Zhang, L.; Lu, T.; Sun, H.; Bridgmohan, C. N.; Weerasinghe, K. C.; Liu, D.; Hu, W.; Li, W.; Zhou, X.; Wang, L. *J. Phys. Chem. C* **2016**, *120*, 25263.
(93) Wang, T.; Weerasinghe, K. C.; Sun, H.; Hu, X.; Lu, T.; Liu, D.; Hu, W.; Li, W.; Zhou, X.; Wang, L. *J. Phys. Chem. C* **2016**, *120*, 11338.
(94) Walkup, L. L.; Weerasinghe, K. C.; Tao, M.; Zhou, X.; Zhang, M.; Liu, D.; Wang, L. *J. Phys. Chem. C* **2010**, *114*, 19521.
(95) Zhou, X.; Liu, D.; Wang, T.; Hu, X.; Guo, J.; Weerasinghe, K. C.; Wang, L.; Li, W. *J. Photochem. Photobiol. A: Chem.* **2014**, *274*, 57.
(96) Wang, T.; Weerasinghe, K. C.; Ubaldo, P. C.; Liu, D.; Li, W.; Zhou, X.; Wang, L. *Chem. Phys. Lett.* **2015**, *618*, 142.
(97) Weerasinghe, K. C.; Wang, T.; Zhuang, J.; Liu, D.; Li, W.; Zhou, X.; Wang, L. *Comput. Mater. Sci.* **2017**, *126*, 244.
(98) Yang, J.; Liu, D.; Lu, T.; Sun, H.; Li, W.; Testoff, T. T.; Zhou, X.; Wang, L. *Int. J. Quantum Chem.* **2020**, *120*, e26355.
(99) Sun, H.; Liu, D.; Wang, T.; Lu, T.; Li, W.; Ren, S.; Hu, W.; Wang, L.; Zhou, X. *ACS Appl. Mater. Interfaces* **2017**, *9*, 9880.
(100) Gong, K.; Xu, F.; Zhao, Z.; Li, W.; Liu, D.; Zhou, X.; Wang, L. *Phys. Chem. Chem. Phys.* **2023**, *25*, 22002.
(101) Wang, T.; Liu, M.; Feng, W.; Cao, R.; Sun, Y.; Wang, L.; Liu, D.; Wang, Y.; Wang, T.; Hu, W. *Adv. Opt. Mater.* **2023**, 2202613.
(102) Liang, Y.; Liu, M.; Wang, T.; Mao, J.; Wang, L.; Liu, D.; Wang, T.; Hu, W. *Adv. Mater.* **2023**, 2304820.
(103) Weerasinghe, K. C.; Wang, T.; Zhuang, J.; Sun, H.; Liu, D.; Li, W.; Hu, W.; Zhou, X.; Wang, L. *Chem. Phys. Impact* **2022**, *4*, 100062.
(104) Beinert, H.; Holm, R. H.; Munck, E. *Science* **1997**, *277*, 653− 659.
(105) Hudson, J. M.; Heffron, K.; Kotlyar, V.; Sher, Y.; Maklashina, E.; Cecchini, G.; Armstrong, F. A. *J. Am. Chem. Soc.* **2005**, *127*, 6977.
(106) Jang, S. B.; Seefeldt, L. C.; Peters, J. W. *Biochem.* **2000**, *39*, 14745−14752.
(107) Fonseca, J. P.; Lee, H.; Boschiero, C.; Griffiths, M.; Lee, S.; Zhao, P.; York, L. M.; Mysore, K. S. *Plant Physiol.* **2020**, *184*, 1532.
(108) Lukianova, O. A.; David, S. S. *Curr. Opin. Chem. Biol.* **2005**, *9*, 145−151.
(109) Kiley, P. J.; Beinert, H. *Curr. Opin. Microbiol.* **2003**, *6*, 181−185.
(110) Ibrahim, I. M.; Wu, H.; Ezhov, R.; Kayanja, G. E.; Zakharov, S. D.; Du, Y.; Tao, W. A.; Pushkar, Y.; Cramer, W. A.; Puthiyaveeti, S. *Commun. Biol.* **2020**, *3*, 13.
(111) Berkovitch, F.; Nicolet, Y.; Wan, J. T.; Jarrett, J. T.; Drennan, C. L. *Science* **2004**, *303*, 76−79.
(112) Wu, C.; Wang, L.; Xiao, Z.; Li, G.; Wang, L. *Chem. Phys. Lett.* **2020**, *746*, 137229.

(113) Wu, C.; Wang, L.; Xiao, Z.; Li, G.; Wang, L. *Phys. Chem. Chem. Phys.* **2020**, *22*, 724.
(114) Wu, C.; Xiao, Z.; Wang, L.; Li, G.; Zhang, X.; Wang, L. *Catal. Sci. Technol.* **2021**, *11*, 1965.
(115) Wu, R.; Sun, K.; Chen, Y.; Zhang, M.; Wang, L. *Surf. Sci.* **2021**, *703*, 121742.
(116) Wu, R.; Wiegand, K. R.; Wang, L. *J. Chem. Phys.* **2021**, *154*, 054705.
(117) Wu, R.; Wiegand, K. R.; Ge, L.; Wang, L. *J. Phys. Chem. C* **2021**, *125*, 14275.
(118) Wu, R.; Wang, L. *Chem. Phys. Impact* **2021**, *3*, 100040.
(119) Wu, R.; Wang, L. *ChemPhysChem* **2022**, *23*, e202200132.
(120) Wu, R.; Wang, L. *Phys. Chem. Chem. Phys.* **2023**, *25*, 2190.
(121) Wu, R.; Wang, L. *J. Phys. Chem. C* **2022**, *126*, 21650.
(122) Wu, R.; Wang, L. *J. Phys. Chem. C* **2020**, *124*, 26953.
(123) Wu, Z.; Zhang, M.; Jiang, H.; Zhong, C.-J.; Chen, Y.; Wang, L. *Phys. Chem. Chem. Phys.* **2017**, *19*, 15444.
(124) Miao, B.; Wu, Z.; Xu, H.; Zhang, M.; Chen, Y.; Wang, L. *Chem. Phys. Lett.* **2017**, *688*, 92.
(125) Miao, B.; Wu, Z.-P.; Xu, H.; Zhang, M.; Chen, Y.; Wang, L. *Comput. Mater. Sci.* **2019**, *156*, 175.
(126) Wang, L.; Ore, R. M.; Jayamaha, P. K.; Wu, Z.-P.; Zhong, C.-J. *Faraday Discuss.* **2023**, *242*, 429.
(127) Wu, R.; Wang, L. *Comput. Mater. Sci.* **2021**, *196*, 110514.
(128) Wu, R.; Wang, L. *Chem. Phys. Lett.* **2017**, *678*, 196.
(129) Perdewa, J. P.; Ruzsinszkya, A.; Sunc, J.; Nepala, N. K.; Kaplana, A. D. *PNAS* **2021**, *118*, e2017850118.
(130) Ali, M. E.; Datta, S. N. *J. Phys. Chem. A* **2006**, *110*, 2776.
(131) Sinnecker, S.; Neese, F.; Noodleman, L.; Lubitz, W. *J. Am. Chem. Soc.* **2004**, *126*, 2613.
(132) Ferre, N.; Guihery, N.; Malrieu, J.-P. *Phys. Chem. Chem. Phys.* **2015**, *17*, 14375.
(133) Neese, F. *J. Phys. Chem. Solid* **2004**, *65*, 781.
(134) Noodleman, L.; Case, D. A.; Aizman, A. *J. Am. Chem. Soc.* **1988**, *110*, 1001.